Topic: TH-C

Fuel supply and helium ash exhaust in global gyrokinetic ITG/TEM turbulence

K. Imadera, Y. Kishimoto, and A. Ishizawa

Graduate School of Energy Science, Kyoto University, Uji, Kyoto 611-0011, Japan
E-mail contact of main author: imadera.kenji.7z@kyoto-u.ac.jp

We perform gyrokinetic flux-driven ITG/TEM simulations to study the balance of fuel supply and helium ash exhaust in tokamaks. It is found that the temperature ratio of helium to bulk ion, i.e. T_{z0}/T_{i0} is one of key parameters to control both fuel supply and helium ash exhaust. For a thermalized helium $T_{z0}/T_{i0}=1$, we observe clear turbulent particle pinch of bulk ions, while turbulent net particle flux of helium is relatively small. On the other hand, for a non-thermalized helium $T_{z0}/T_{i0}=4$, such a turbulent particle pinch of bulk ions is found to be weekend and helium ash accumulation occurs because turbulent particle flux of helium by non-axisymmetric radial drift tends to become negative. This means that hot helium can prevent both fuel supply and helium ash exhaust.

Establishment of a refueling method is an important issue to control nuclear fusion reactors. But, in DEMO-class high-temperature plasmas, a pellet injection reaches only up to 80-90% of the minor radius so that the central density peaking depends on particle pinch, making the prediction difficult. While turbulent particle transport has been studied based on mainly local gyrokinetic models [1], it is also important to study global effects such as profile shearing, mean flow, and the interplay between neoclassical and turbulent transport. The above analysis is also meaningful to investigate impurity transport such as core helium ash exhaust and edge impurity accumulation [2]. Based on such a motivation, we investigate the balance of fuel supply and helium ash exhaust by means of full-*f* gyrokinetic code GKNET with hybrid electron model [3]. Unlike some simplified transport models, the full-*f* gyrokinetic model enables us to simulate flux-driven turbulence consistently coupled with a neoclassical transport mechanism, which is a novelty of this work.

Figure 1 (a) shows the bulk ion density profiles after the nonlinear saturation in the two flux-driven ITG/TEM simulations, which initial temperature gradients are given by $\left(R_0/L_{T_i}, R_0/L_{T_e}, R_0/L_{T_z}\right)=(10,10,10)$ under both ion and electron heating, and $\left(R_0/L_{T_i}, R_0/L_{T_e}, R_0/L_{T_z}\right)=(10,4,10)$ under ion heating, respectively. The deposition profiles of applied heat source and energy sink are also shown. Here, 90% hydrogen and 10% helium are applied as the bulk ion and impurity. It is found that clear bulk ion density peaking is found to be observed in the ion/electron heating case, while density profile is weakly relaxed in the ion heating case. The temporal evolutions of non-axisymmetric and axisymmetric turbulent ion particle fluxes in the ion/electron heating and ion heating cases are shown in Fig. 1 (b) and (c), respectively. As was found from the flux-driven ITG/TEM simulations in the absence of impurities [4], ion heating can drive turbulent ion particle pinch by non-axisymmetric drift (see the red lines in Fig. 1 (b) and (c)). In addition, electron heating can also drive turbulent electron particle pinch by non-axisymmetric drift due to the phase gap between trapped electron density perturbation and electrostatic potential, which can trigger an ambipolar electric field, leading to additional ion particle pinch by axisymmetric drift (see the blue line in Fig. 1 (b)). These results suggest that a density peaking of bulk ion due to turbulent fluctuations can be achieved by sufficiently strong both ion and electron heating even in the presence of impurities.

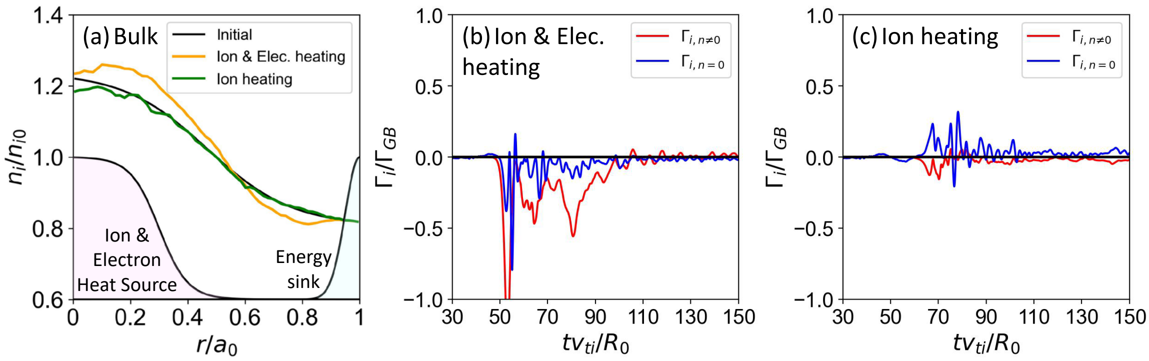

Fig. 1: (a) Bulk ion density profiles after the nonlinear saturation ($tv_{ti}/R_0=150$) in the ion/electron heating (yellow), and ion heating (green) cases, respectively. Temporal evolutions of non-axisymmetric (red) and axisymmetric (blue) turbulent ion particle fluxes in the (b) ion/electron heating and (c) ion heating cases.

Figure 2 (a) shows the helium density profiles after the nonlinear saturation in the two flux-driven ITG/TEM simulations. The temporal evolutions of non-axisymmetric and axisymmetric turbulent particle fluxes of helium in the ion/electron heating and ion heating cases are also shown in Fig. 2 (b) and (c), respectively. It is found that turbulent particle flux of helium by non-axisymmetric radial drift can provide helium ash exhaust (see the red lines in Fig. 2 (b) and (c)) contrary to the tendency of turbulent particle flux of bulk ion. However, turbulent particle flux of helium by axisymmetric one is found to become negative in the ion/electron heating case (see the blue lines in Fig. 2 (b)) because turbulent particle transport triggers up-down asymmetric density perturbations, which enhance the Banana-Plateau flux. Note that such a contribution is not considered in local and global δf simulations. As the result, these two fluxes cancel with each other and total net particle flux of helium becomes small in the ion/electron heating case. In the ion heating case, by contrast, turbulent particle flux of helium by axisymmetric one is weakly positive, leading to the helium ash exhaust.

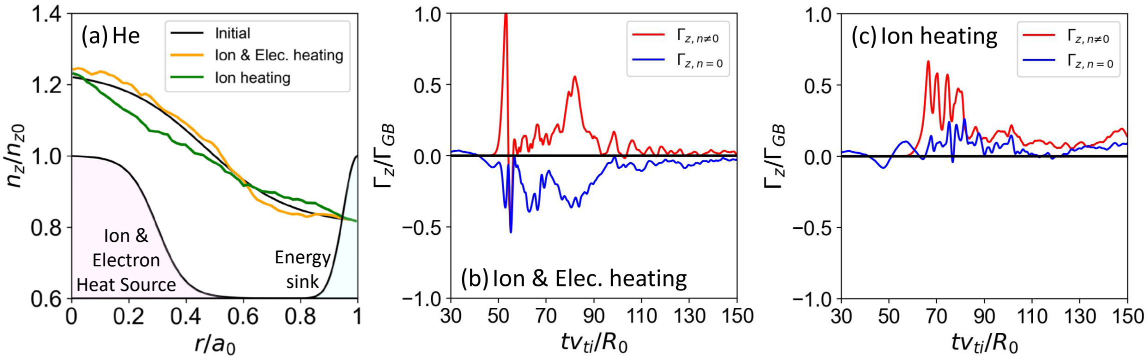

Fig. 2: (a) Helium density profiles after the nonlinear saturation ($tv_{ti}/R_0 = 150$) in the ion/electron heating (yellow), and ion heating (green) cases, respectively. Temporal evolutions of non-axisymmetric (red) and axisymmetric (blue) turbulent particle fluxes of helium in the (b) ion/electron heating and (c) ion heating cases.

Then, we change the temperature ratio of helium to bulk ion; T_{z0}/T_{i0}. Figure 3 shows (a) bulk ion and (b) helium density profiles after the nonlinear saturation in the ion/electron heating case with $T_{z0}/T_{i0} = 1$ (same as the yellow line in Fig. 1 (a) and Fig. 2(a)) and $T_{z0}/T_{i0} = 4$. Interestingly, once the helium temperature increases, turbulent particle flux of helium by non-axisymmetric radial drift tends to become negative, leading the density peaking of helium (see the purple line in Fig. 3 (b)). Figure 4 shows the net particle pinch of bulk ion and helium normalized by that in the case with $T_{z0}/T_{i0} = 1$. This result demonstrates that the hot helium, i.e. higher T_{z0}/T_{i0} can prevent both fuel supply and helium ash exhaust, indicating the temperature ratio of helium to bulk ion is one of key parameters to control them.

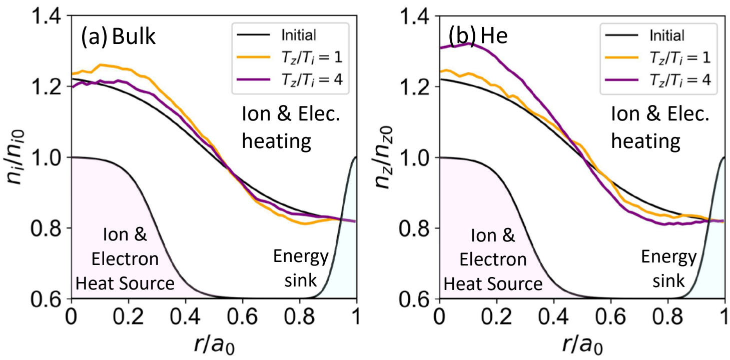

Fig. 3: (a) Bulk ion $n_i(r)$ and (b) helium $n_z(r)$ density profiles after the nonlinear saturation ($tv_{ti}/R_0 = 150$), where initial temperature gradients are given by $(R_0/L_{T_i}, R_0/L_{T_e}, R_0/L_{T_z}) = (10, 10, 10)$ under ion and electron heating with $T_{z0}/T_{i0} = 1$ (yellow) and $T_{z0}/T_{i0} = 4$ (purple).

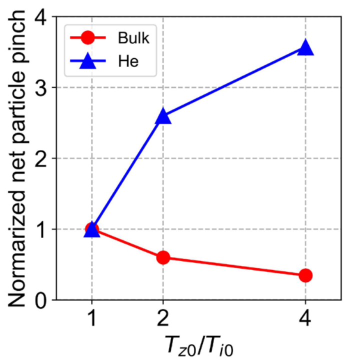

Fig. 4: Net particle pinch of bulk ion (red) and helium (blue) normalized by that in the case with $T_{z0}/T_{i0} = 1$. Initial temperature gradients are given by $(R_0/L_{T_i}, R_0/L_{T_e}, R_0/L_{T_z}) = (10, 10, 10)$ under ion and electron heating.

[1] C. Angioni *et al.*, Plasma Phys. Control. Fusion **51**, 124017 (2009).
[2] C. Angioni *et al.*, Plasma Phys. Control. Fusion **63**, 073001 (2021).
[3] K. Imadera *et al.*, Plasma Phys. Control. Fusion **65**, 024003 (2023).
[4] K. Imadera *et al.*, Nucl. Fusion **64**, 086006 (2024).